

# Effect of iodine contrast agent concentration on cerebrovascular dose for synchrotron radiation microangiography based on a simple mouse head model and a voxel mouse head phantom by Monte Carlo simulation

Hui Lin,<sup>a\*</sup> Jia Jing,<sup>a</sup> Yi-Fan Lu,<sup>b</sup> Cong Xie,<sup>a</sup> Xiao-Jie Lin<sup>b</sup> and Guo-Yuan Yang<sup>b</sup>

Received 21 April 2015  
Accepted 9 October 2015

Edited by A. Momose, Tohoku University, Japan

**Keywords:** synchrotron radiation microangiography; irradiation dose damage; Monte Carlo simulation.

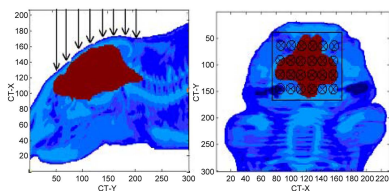
<sup>a</sup>School of Electronic Science and Application Physics, Hefei University of Technology, 230009 Hefei, People's Republic of China, and <sup>b</sup>Neuroscience and Neuroengineering Centre, Med-X Research Institute and School of Biomedical Engineering, Shanghai Jiao Tong University, Shanghai 200030, People's Republic of China.

\*Correspondence e-mail: huilin@hfut.edu.cn

Effective setting strategies using Monte Carlo simulation are presented to mitigate the irradiation damage in synchrotron radiation microangiography (SRA). A one-dimensional mouse head model and a segmented voxel phantom mouse head were simulated using the *EGSnrc/DOSXYZnrc* code to investigate the dose enhancement effect of an iodine contrast agent irradiated by a monochromatic synchrotron radiation source. The influence of the iodine concentration, vessel width and depth, protection with and without the skull layer, and various incident X-ray energies were all simulated. The dose enhancement effect and the absolute dose based on the segmented voxel mouse head phantom were evaluated. The dose enhancement ratio depended little on the irradiation depth, but strongly and linearly increasing on iodine concentration. The protection given by the skull layer cannot be ignored in SRA because a 700  $\mu\text{m}$ -thick skull can decrease the dose by 10%. The incident X-ray energy can affect the dose significantly. Compared with a dose of 33.2 keV for 50 mgI ml<sup>-1</sup>, a dose of 32.7 keV decreased by 38%, whereas a dose of 33.7 keV increased by 69.2% and the variation strengthened more with enhanced iodine concentration. The segmented voxel mouse head phantom also showed that the average dose enhancement effect and the maximal voxel dose per photon depended little on the iodine voxel volume ratio but strongly on the iodine concentration. To decrease the damage caused by the dose in SRA, a high-Z contrast agent should be used as little as possible and irradiation of the injection site of the contrast agent should be avoided immediately after the injection. The fragile vessel containing iodine should avoid being closely irradiated. Avoiding irradiating through a thin (or no) skull region, or attaching a thin equivalent material on the outside for protection are better methods. An incident X-ray energy as low as possible should be used as long as the SRA image quality is ensured. The use of the synergetic and synchronous shuttering technique in SRA is also very critical in order to effectively shorten the accumulative irradiation time in *in vivo* animal irradiation experiments.

## 1. Introduction

Synchrotron radiation microangiography (SRA) provides a unique tool for monitoring hemodynamic changes and microvascular morphology owing to its high brilliance and extreme collimation, allowing enhanced sensitivity to contrast material and superior image quality in terms of spatial and density resolution (Schwenke *et al.*, 2008). Compared with conventional X-rays, synchrotron radiation X-rays can be used to generate images of higher quality (Keyriläinen *et al.*, 2008)



and make possible the early detection of small lesions (Castelli *et al.*, 2011). Recent developments have shown that SRA could be utilized for high-resolution imaging of cerebral vasculature (Kidoguchi *et al.*, 2006; Lu *et al.*, 2012; Yuan *et al.*, 2011). Laser speckle contrast imaging (LSCI) has been used to monitor blood flow and cortical collateral arteries after ischemic stroke (Ayata *et al.*, 2013; Wang *et al.*, 2012).

Many works have used iodine contrast agents such as Iomeprol<sup>®</sup>, Iomeron<sup>®</sup> and Iopamiro to provide good contrast and minimal distortion of the circulation and the vessel structure (Chien *et al.*, 2010; Kidoguchi *et al.*, 2006; Lin, Miao *et al.*, 2013). Kidoguchi *et al.* (2006) have performed *in vivo* X-ray angiography in a mouse brain at SPring-8 (a third-generation synchrotron radiation facility). They used a thin PE-50 tube to deliver 33  $\mu\text{l}$  of nonionic iodine contrast agent to the brain of C57BL/6J mice and found that the morphology of the vessels can be clearly observed under physiological conditions. Lin, Miao *et al.* (2013) used LSCI to investigate the relationship between focal thrombus formation and model reproducibility with respect to infarct volume, to determine whether or not suture insertion causes thrombus formation and influences the success of reperfusion and collateral circulation during the reperfusion period in mice using the transient middle cerebral artery occlusion model. Chien *et al.* (2010) used microemulsions of the hydrophobic contrast agent Lipiodol<sup>®</sup> and gold nanoparticles to visualize small ( $<8 \mu\text{m}$ ) vessels in mice tumor-related microangiogenesis.

However, some works have found that animals, such as mice and rats, could not survive for an extended period after angiography owing to radiation injury or the toxicity of a relatively large volume of contrast agent (*e.g.* 300–500  $\mu\text{l}$  for rats and 80  $\mu\text{l}$  for mice) (Lin, Miao *et al.*, 2013; Longo *et al.*, 2002; Piepgras *et al.*, 1995). Owing to the high brilliance of synchrotron sources, in the irradiated setting of an SRA experiment it is very critical to be able to decrease the irradiated dose and to increase the survival rate of the mice. Thus, with respect to the current conventional setting (*i.e.* being rigidly held on a frame, vertically and statically to the radiation beam and immediate microangiography after contrast agent injection *etc.*), only when a practical solution is found to control the radiation dose can SRA be used to visualize the entire process of cerebral blood flow longitudinally (Lin, Miao *et al.*, 2013).

Monte Carlo simulation is generally considered as the most accurate method due to its ability to model the geometry and the physical interaction between radiation and matter (Saltybaeva *et al.*, 2014). The Monte Carlo method can also be regarded as a dose evaluation tool to optimize for the irradiation scheme of cancer radiotherapy (Lin, Cai *et al.*, 2013), radionuclide therapy (Lin *et al.*, 2012) or angiography (Deak *et al.*, 2010; Saltybaeva *et al.*, 2014).

This work studies the dose enhancement effect of an iodine contrast agent on the cerebral vessel dose for SRA based on a 1-D mouse head model and a segmented voxel mouse head phantom by Monte Carlo simulation. Some useful suggestions about the setting strategy for an SRA experiment to mitigate irradiation dose damage are given.

## 2. Materials and methods

### 2.1. A 1-D mouse head model

The 1-D mouse head model (1-D MHM) is assumed to be composed of a 500  $\mu\text{m}$  skin layer, a 700  $\mu\text{m}$  skull layer and a 0.6 cm brain layer. These sizes are chosen with reference to the structure of a 3D mouse atlas model (Dogdas *et al.*, 2007; Stout *et al.*, 2002). The 1-D MHM can be adjusted to investigate the influence of different layer thicknesses. The basic iodine vessel layer (IVL) containing iodine solution is assumed to be located at 500  $\mu\text{m}$  behind the skull layer, which is equivalent to the skin thickness. According to measurements based on synchrotron radiation LSCI microangiography, the average middle cerebral artery diameter is around  $142.5 \pm 7.90 \mu\text{m}$  (Kidoguchi *et al.*, 2006) or  $134.0 \pm 7.21 \mu\text{m}$  (Miao *et al.*, 2014), and the average common carotid artery (CCA) diameter is around  $500 \pm 20 \mu\text{m}$  (Ota *et al.*, 2009). We assume the IVL thickness in the 1-D MHM is 200  $\mu\text{m}$  and can vary up to 500  $\mu\text{m}$ .

### 2.2. A mouse head voxel phantom

The Digimouse 3D mouse atlas model was used as a voxel mouse head phantom (VMHP). The Digimouse atlas was generated using coregistered computed tomography (CT) and cryosection images of a 28 g nude normal male mouse of matrix size  $380 \times 992 \times 208$  with 0.1 mm cubic voxels. The structures segmented from these data include: whole brain, external cerebrum, cerebellum, olfactory bulbs, striatum, medulla, masseter muscles, skin and other organs. The CT identifier of the head is located at  $X = [70, 300]$ ,  $Y = [600, 900]$  and  $Z = [1, 208]$ , *i.e.* its matrix size is  $230 \times 300 \times 208$ . Its brain is located at  $X = [143, 238]$ ,  $Y = [687, 860]$  and  $Z = [89, 162]$ .

### 2.3. Synchrotron radiation source

The radiation source is assumed to be a synchrotron radiation source, *e.g.* the X-ray imaging beamline BL13W at the Shanghai Synchrotron Radiation Facility (SSRF). The parallel monochromatic X-ray energy is 33.2 keV, which is just above the iodine *K*-edge energy and is often used in microangiography with an iodine contrast agent. The irradiation field is up to 45 mm (H)  $\times$  4.5 mm (W) for a single field (Lin, Miao *et al.*, 2013).

### 2.4. Iodine concentration

The contrast agent Iopamiro (80  $\mu\text{l}$ , 175 mgI  $\text{ml}^{-1}$ , Iopamiro, Shanghai, China) is injected into the CCA at a rate of 33.3  $\mu\text{l s}^{-1}$  and the angiography is performed immediately to visualize the high flow ability of the bloodstream with the iodine contrast agent (Lin, Miao *et al.*, 2013; Miao *et al.*, 2014). The iodine concentration (IC) in the vessels can be expected to vary from 0 to 175 mgI  $\text{ml}^{-1}$ . The maximum value of 175 mgI  $\text{ml}^{-1}$  represents the extreme situation because the contrast agent is injected just at the beginning and there is not enough time for it to flow. Thus, the local IC can reach a high value.

2.5. Monte Carlo method

The Monte Carlo program *EGSnrc* simulates the transport of photons and electrons in a generalized rectilinear or cylindrical volume. It incorporates significant improvements in implementing the condensed history technique for the charged particle transport and better low-energy cross sections (Kawrakow *et al.*, 2010). Its electron and photon cut-off energies can be low, a little more than 511 keV for electrons [*i.e.* greater than the electron rest energy (AE) of 511 keV] and 1 keV for photons. The user code *DOSXYZnrc* simulates the particle transport in a Cartesian volume and scores the energy deposition in designated voxels. The *DOSXYZnrc* geometry is a rectilinear volume composed of voxels. The voxel dimensions are completely variable in all three directions and each voxel can be designated different materials and/or varying densities for use with CT data (Walters *et al.*, 2011).

The 1-D MHM is assumed to be 5 cm × 5 cm × 0.72 cm for its small irradiation field [45 mm (H) × 4.5 mm (W)]; the small thickness in the Z direction is to reduce the simulation time of the particle transport. The voxel size is assumed to be 1 cm × 0.1 cm × 0.01 cm. The small voxel thickness in the Z direction allows for the tiny size of the mouse; however, the relatively large size in the X direction is to increase the voxel score volume and decrease the statistical uncertainty.

The VMHP computed tomograph, except for the brain, was converted into four types of materials by the *EGSnrc* utility program *ctcreate*, *i.e.* AIR521ICRU, LUNG521ICRU, ICRU-TISSUE521ICRU and ICRPBONE521ICRU. Their densities vary with different CT values, for example, 0.001–0.044 g cm<sup>-3</sup> for AIR521ICRU with CT [0, 50], 0.044–0.302 g cm<sup>-3</sup> for LUNG521ICRU with CT [50, 300], 0.302–1.101 g cm<sup>-3</sup> for ICRUTISSUE521ICRU with CT [300, 1125] and 1.101–2.088 g cm<sup>-3</sup> for ICRPBONE521ICRU with CT [1125, 3000]. The brain voxel is designated by a specific material called BrainICRU44 with a fixed density of 1.04 g cm<sup>-3</sup>. The brain vessel that was not segmented in the mouse atlas model was assumed to be selected stochastically and controlled by the volume ratio of the voxel incorporating iodine (VI) to the whole brain (*e.g.* 2, 4, 6, 8 and 10%). The VI was filled by a sixth material, WaterNmgmI521 (*i.e.* water incorporating *N* mg ml<sup>-1</sup> iodine; here *N* represents the concentration value with units of mg ml<sup>-1</sup> in water).

The material data of WaterNmgmI521 and BrainICRU44 were produced by *PEGS4* (the preprocessor for *EGSnrc*), which is a stand-alone utility program aimed at generating material data for *EGSnrc*. The low cutoff energies for charged particle transport, AE = 521 keV, and photon transport, AP = 1 keV, were used, which correspond to electron and photon cutoff kinetic energies of 1 keV. Both the globe electron and photon cutoffs (ECUT and PCUT) were set to equal AE and

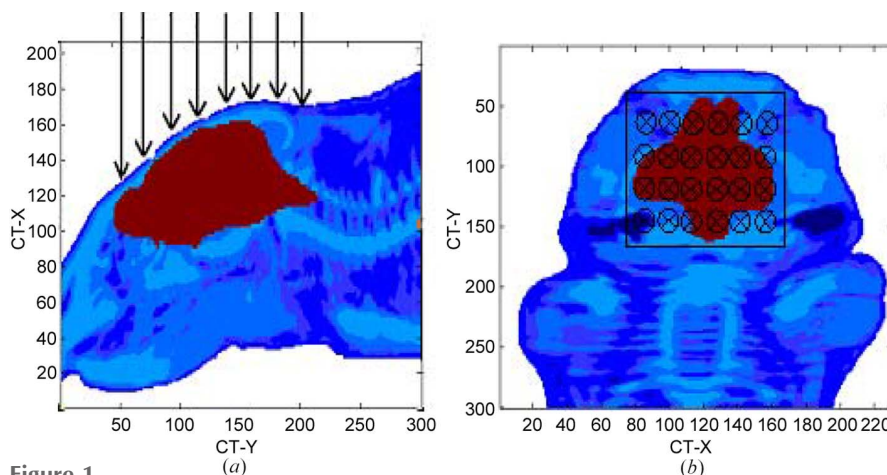


Figure 1 (a) Sectional density map and (b) irradiation field of the VMHP.

AP, respectively. The PRESTA-II algorithm has been employed for the electron step control, which takes into account the lateral and the longitudinal correlations in the condensed history step.

To perform whole brain microangiography in the VMHP, the irradiation field has to cover the whole brain. Here, we assume the synchrotron radiation beam irradiates the whole atlas brain vertically from the tritocerebrum direction with a 10 mm × 20 mm field, which can be performed by scanning with a narrow beam of synchrotron radiation. To calculate the absolute dose, the X-ray flux per sectional area 6 × 10<sup>9</sup> photons s<sup>-1</sup> mm<sup>-2</sup> at 32 keV using Si(111) of the SSRF, was used. The irradiation field still is 45 mm (H) × 4.5 mm (W) for the 1-D MHM. Fig. 1 shows the sectional density map and the irradiation field of the VMHP.

3. Results

Fig. 2(a) shows depth dose curves (DDCs) for the 1-D MHM irradiated with X-rays of energy 33.2 keV. The dose in the skull layer is almost sevenfold greater than that in the brain due to its higher-Z elements and higher physical interaction cross section (*i.e.* photoelectric effect and Compton scattering effect, *etc.*). The dose in the iodine vessel layer also increases with increasing IC for the same reasons. The DDCs decrease slightly with increasing depth in the IVL for a certain IC and decrease more for a higher IC.

To study the influence of different IVL thicknesses, Fig. 2(b) shows the DDCs with a 500 μm IVL (comparable with the CCA) in the 1-D MHM. The DDCs decrease more in the wider IVLs. Fig. 2(c) shows the variation of the dose enhancement ratio (DER) with increasing IC at the front and the back depths of the 200 μm and 500 μm IVLs. The dose buildup effect around the IVL interface is about 20 μm (two-voxel thickness here) and the compared DER depths are the front-third depth (at 0.173 cm) and back-third depth (at 0.188 cm or 0.218 cm) in the IVL. In general, the DER increases linearly with increasing IC. The relationship between

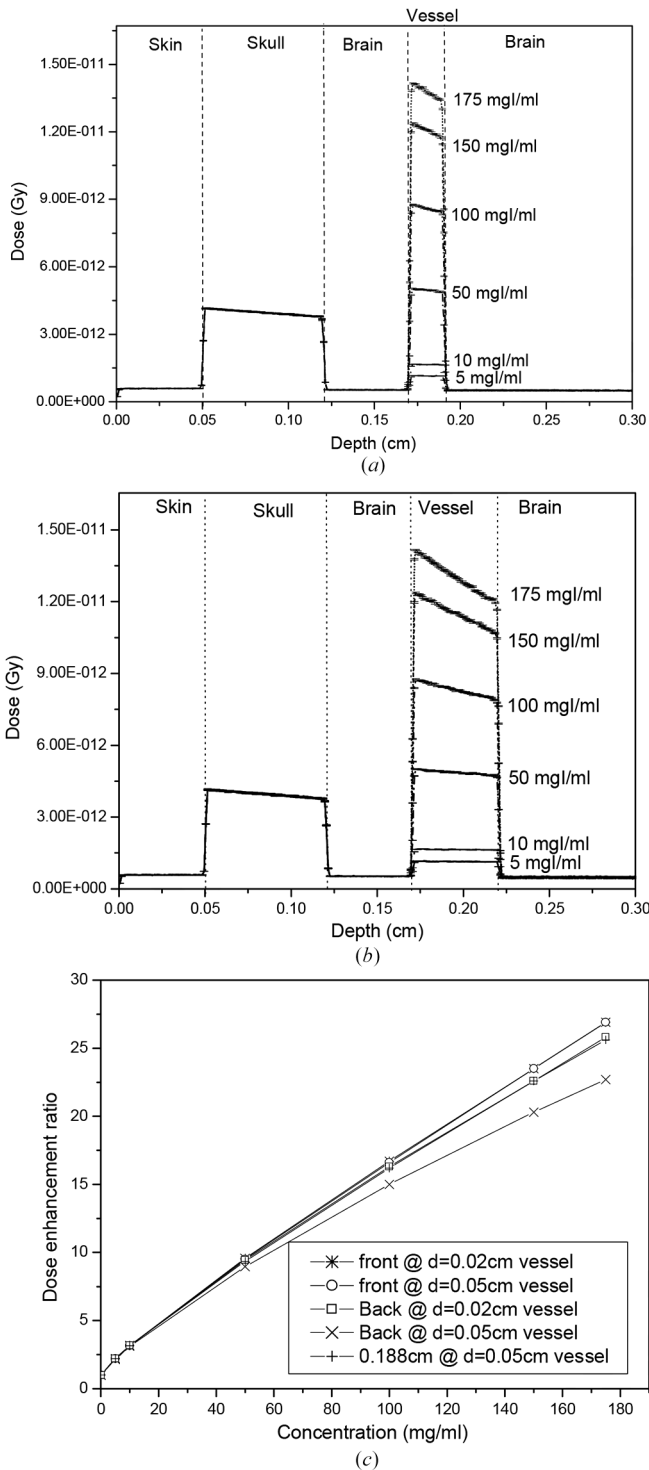


**Figure 2**  
DDC and DER for 200 μm and 500 μm IVLs with different ICs: (a) DDC for 200 μm IVL, (b) DDC for 500 μm IVL, (c) DER for 200 μm and 500 μm IVLs.

DER and IC can be fitted by a linear equation. For example, the DER with IC at 0.188 cm depth can be fitted by

$$\text{DER} = 1.0 + 0.1432 \text{IC}, \quad (1)$$

with a goodness of fit  $R^2$  of more than 0.998. For both the 200 μm and the 500 μm interfaces, their same depth DERs are

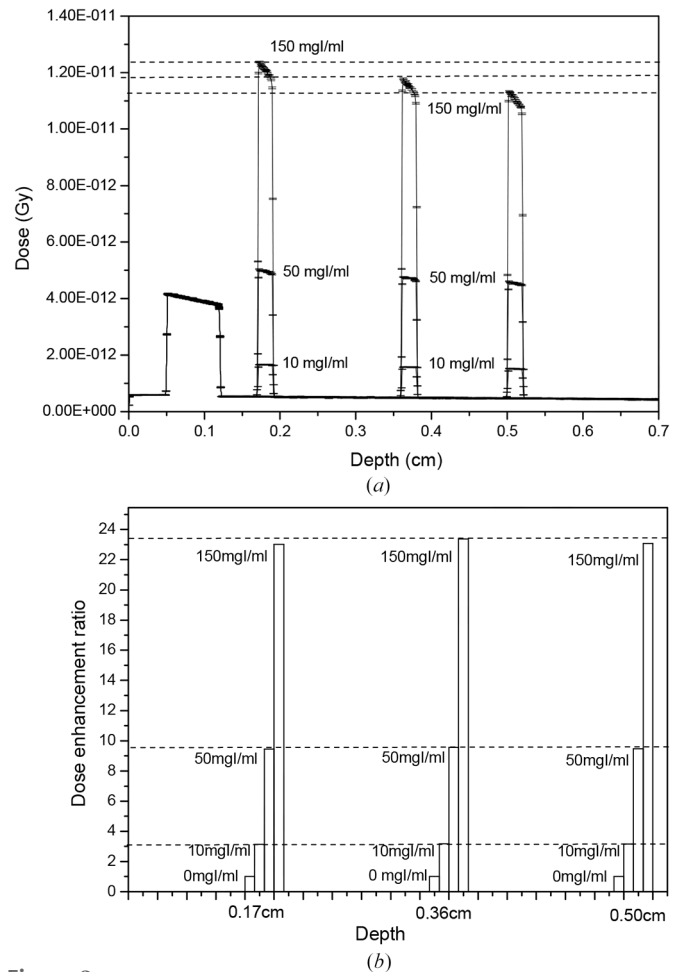


**Figure 3**  
(a) DDC and (b) DER for the 200 μm IVL for different depths and ICs.

approximate (*i.e.* a 0.188 cm depth for the 200 μm and the 500 μm IVLs). The DER decreases slightly with increase in depth for the higher IC. For example, the DER at 0.173 cm depth is  $1.11\times$  that at 0.218 cm depth for  $100 \text{ mgI ml}^{-1}$ ; however, the ratio will increase 1.19 times for  $175 \text{ mgI ml}^{-1}$ .

To study the influence of different depth vessels, the 200 μm IVL is placed at different depths in the 1-D MHM (*e.g.* the distance of the IVL front from the 1-D MHM surface is 0.17, 0.36 or 0.50 cm). Fig. 3(a) shows DDC comparisons for three different ICs (10, 50 and  $150 \text{ mgI ml}^{-1}$ ). The DDCs decrease slightly with increasing depth, whereas the DERs do not vary much (Fig. 3b).

To study the protection effect of the skull layer, the 1-D MHM without a skull layer was simulated. Fig. 4 shows a comparison of the DDCs with the original 1-D MHM. In general, the dose in the IVL increases by approximately 10%, but the DERs with IC are similar to that of the original 1-D MHM and are not repeated here.

Generally, the incident X-ray energy cannot be accurately set for the medium attenuation in SRA, which makes the hypothetical X-ray energy deviate from the iodine *K*-edge energy. X-ray energies around 33.2 keV in steps of 0.5 keV were simulated. Fig. 5(a) shows the DDCs for different energies (32.7, 33.2, 33.7, 34.2 and 34.7 keV). As the X-ray energy

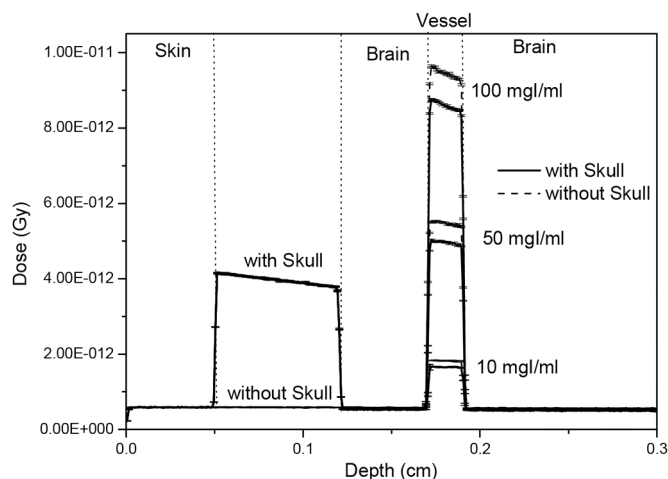


**Figure 4**  
DDCs with and without skull protection.

increases, the dose in the skull decreases slightly (e.g. 3.15% for 33.7 keV, 5.43% for 34.2 keV and 7.85% for 34.7–33.2 keV), whereas the dose in the IVL varies more. Compared with the dose of 33.2 keV for 50 mgI ml<sup>-1</sup>, the 32.7 keV dose decreases to 38%, whereas the doses of 33.7, 34.2 and 34.7 keV increase up to 69.2, 68.1 and 66.3%, respectively. Fig. 5(b) shows a comparison of the DER at different energies with those at 33.2 keV for different ICs.

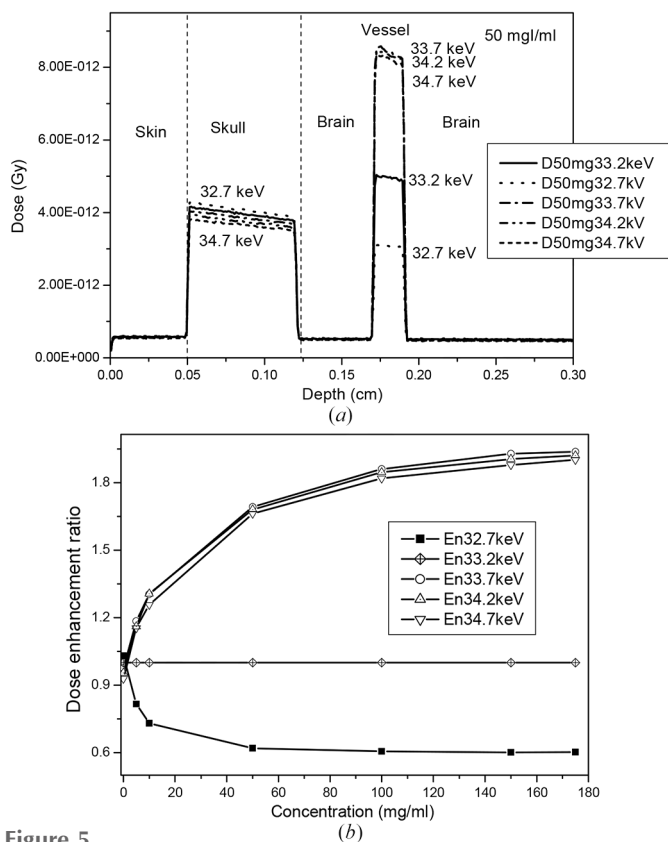


**Figure 5**  
DDC and DER comparison for different energies. (a) DDCs for different energies (32.7, 33.2, 33.7, 34.2 and 34.7 keV) and (b) DER comparison for different energies (32.7, 33.2, 33.7, 34.2 and 34.7 keV) with those of 33.2 keV with different ICs.

Except for the 0 mgI ml<sup>-1</sup> concentration, the DER decreases for lower incident energy (up to approximately 40% for 32.7 keV with >50 mgI ml<sup>-1</sup>) and the DER increases for higher incident energy (up to ~90% for 33.7, 34.2 and 34.7 keV with >50 mgI ml<sup>-1</sup>) with increasing IC. Thus, the iodine contrast agent not only enlarges the difference in the DDC for different energies but also overturns the DER feature in the IVL with increasing IC.

Table 1 shows a comparison of the average DER, the maximal and the average VI dose per photon for different VI volume ratios (VIRs) and the ICs in the VMHP. To consider the widest range of possible VIR conditions, 2–10% of VIRs were simulated. The average DER was obtained based on all the VI DERs in the VMHP. The simulation indicates that the average DER and the maximal VI dose per photon depend little on the VIR but strongly on the IC, which agrees with that of the 1-D MHM. The estimated DER generated from equation (1) is also given in Table 1. Generally there is good coincidence for  $\leq 50$  mgI ml<sup>-1</sup>, but there is a relatively larger difference for 100 mgI ml<sup>-1</sup>. This is because equation (1) was obtained based on a certain depth (0.188 cm) in the 1-D MHM, but the average DER was obtained based on all depths in the VMHP. The 1-D MHM simulation also shows that the DER increase will decrease with increasing depth for high IC (Fig. 2c).

Although the maximal VI dose is located at different positions in the VMHP for different VIRs and ICs, their values are very approximate for the same IC (less than 5%). The maximal VI dose per photon represents the dose hot spot, as well as the dangerous spot for SRA. If the proportion of the maximal to the average VI dose reflects the dose uniformity, the simulation indicates that the IC increase improves the dose uniformity.

Table 2 presents the maximal and the average absolute dose per second, and the corresponding tolerance radiation time (TRT) for a tolerance dose (TD) of 15 Gy for TD5/5 (5% chance of injury showing up over the next five years) and 25 Gy for TD50/5 (50% chance of an injury) based on the human brain irradiated by a single dose (Emami *et al.*, 1991). The photon flux is assumed to be  $6 \times 10^9$  photons s<sup>-1</sup> mm<sup>-2</sup> as found at the SSRF. Dynamic images are assumed to be obtained from a PCO X-ray CCD camera (PCO-TECH Inc., Germany) at a rate of 7 frames s<sup>-1</sup> (Lin, Cai *et al.*, 2013). Generally the shutter open time is 10–20 ms frame<sup>-1</sup> (here a higher value of 20 ms frame<sup>-1</sup> is assumed for caution). Sometimes the shutter is not used in SRA for operation inconvenience (e.g. in operating the rotation linkage between sample, detector and shutter *etc.*), thus in this situation the synchrotron radiation source will be working and passing through the rat during the image shooting and storage time. If the brain vessel is assumed to be a serial-like structure, its TRT is determined by TD5/5 or TD50/5 divided by the maximal voxel dose. The TRT determined by TD5/5 or TD50/5 divided by the average voxel dose, which is generally applicable for parallel-like structures such as the brain, is also shown for reference. Table 2 presents a comparison of TRT for TD5/5 and TD50/5 with and without shutter control for the VMHP.

**Table 1**  
Comparison of the average DER for different VIRs and ICs for the VMHP.

The photon flux is assumed to be  $6 \times 10^9$  photons  $s^{-1} mm^{-2}$  at 32 keV using Si(111), as at the SSRF.

VIR (%)	IC (mgI ml <sup>-1</sup> )				
	0	5	10	50	100
DER					
2	1	1.85 ± 0.077	2.61 ± 0.123	7.51 ± 0.404	12.92 ± 0.770
4	1	1.86 ± 0.077	2.61 ± 0.125	7.49 ± 0.409	12.85 ± 0.781
6	1	1.86 ± 0.077	2.61 ± 0.126	7.48 ± 0.414	12.78 ± 0.804
8	1	1.86 ± 0.079	2.61 ± 0.128	7.47 ± 0.428	12.71 ± 0.839
10	1	1.86 ± 0.080	2.62 ± 0.130	7.45 ± 0.441	12.64 ± 0.878
1-D MHM	1	1.71	2.432	8.16	15.32
Maximal and average VI dose per photon					
2	1.07 × 10 <sup>-12</sup> / 1.5% 6.20 × 10 <sup>-13</sup>	1.67 × 10 <sup>-12</sup> / 2.1% 1.14 × 10 <sup>-12</sup>	2.23 × 10 <sup>-12</sup> / 2.3% 1.59 × 10 <sup>-12</sup>	5.68 × 10 <sup>-12</sup> / 1.7% 4.59 × 10 <sup>-12</sup>	9.71 × 10 <sup>-12</sup> / 2.3% 7.90 × 10 <sup>-12</sup>
4	1.07 × 10 <sup>-12</sup> / 1.6% 6.19 × 10 <sup>-13</sup>	1.67 × 10 <sup>-12</sup> / 2.2% 1.14 × 10 <sup>-12</sup>	2.23 × 10 <sup>-12</sup> / 2.3% 1.60 × 10 <sup>-12</sup>	5.76 × 10 <sup>-12</sup> / 1.6% 4.58 × 10 <sup>-12</sup>	9.80 × 10 <sup>-12</sup> / 2.3% 7.85 × 10 <sup>-12</sup>
6	1.07 × 10 <sup>-12</sup> / 1.6% 6.19 × 10 <sup>-13</sup>	1.68 × 10 <sup>-12</sup> / 2.1% 1.14 × 10 <sup>-12</sup>	2.24 × 10 <sup>-12</sup> / 2.3% 1.60 × 10 <sup>-12</sup>	5.86 × 10 <sup>-12</sup> / 1.7% 4.57 × 10 <sup>-12</sup>	9.93 × 10 <sup>-12</sup> / 2.3% 7.81 × 10 <sup>-12</sup>
8	1.08 × 10 <sup>-12</sup> / 1.5% 6.20 × 10 <sup>-13</sup>	1.69 × 10 <sup>-12</sup> / 2.1% 1.14 × 10 <sup>-12</sup>	2.32 × 10 <sup>-12</sup> / 2.2% 1.60 × 10 <sup>-12</sup>	5.80 × 10 <sup>-12</sup> / 1.7% 4.56 × 10 <sup>-12</sup>	1.00 × 10 <sup>-11</sup> / 2.2% 7.76 × 10 <sup>-12</sup>
10	1.09 × 10 <sup>-12</sup> / 1.5% 6.20 × 10 <sup>-13</sup>	1.72 × 10 <sup>-12</sup> / 2.1% 1.14 × 10 <sup>-12</sup>	2.27 × 10 <sup>-12</sup> / 2.2% 1.60 × 10 <sup>-12</sup>	5.82 × 10 <sup>-12</sup> / 1.6% 4.55 × 10 <sup>-12</sup>	1.00 × 10 <sup>-11</sup> / 2.2% 7.72 × 10 <sup>-12</sup>

**Table 2**  
Comparison of tolerance radiation time for TD5/5 and TD50/5 with and without shutter control for the VMHP.

	IC (mgI ml <sup>-1</sup> )				
	0	5	10	50	100
With shutter control					
Maximum and average dose per second†	182 / 103.6	284.2 / 191.8	379.4 / 268.8	971.6 / 767.2	1661.8 / 1311.8
TRT for TD5/5	82.42 / 144.79	52.78 / 78.21	39.54 / 55.80	15.44 / 19.55	9.03 / 11.43
TRT for TD50/5	137.36 / 241.31	87.97 / 130.34	65.89 / 93.01	25.73 / 32.59	15.04 / 19.06
Without shutter control					
Maximum and average dose per second†	1.30 / 0.74	2.03 / 1.37	2.71 / 1.92	6.94 / 5.48	11.87 / 9.37
TRT for TD5/5	11.54 / 20.27	7.39 / 10.95	5.54 / 7.81	2.16 / 2.74	1.26 / 1.60
TRT for TD50/5	19.23 / 33.78	12.32 / 18.25	9.23 / 13.02	3.60 / 4.56	2.11 / 2.67

† Calculated by the maximal and the average VI dose per photon in Table 1.

In general, the tolerance time without a shutter will be shortened by about six times compared with that with a shutter.

The simulated source particles are  $1 \times 10^9$  for the 1-D MHM with uncertainty <0.5% in the IVL and  $4 \times 10^9$  to  $16 \times 10^9$  for the VMHP with an uncertainty of <2–3% in the VI for its small voxel volume (*i.e.* generally  $16 \times 10^9$  for the VMHP without VIs and  $4 \times 10^9$  to  $8 \times 10^9$  for the VMHP with VIs of different ICs). The simulation time is about 30 h for 1-D MHM and 15 h for VMHP per  $1 \times 10^9$  (*i.e.* the simulation time is about  $4 \times 15$  to  $4 \times 16$  h for the VMHP with VIs of different ICs) using an Intel(R) Xeon(R) E5620 Power (CPU 2.40 GHz, 3.0 GB memory) Windows 32 XP system.

#### 4. Discussion

Synchrotron radiation microangiography, as an innovatory angiography technique, could monitor hemodynamic changes and microvascular morphology because of its high brilliance and collimation, whereas its cooperative usage with high-Z contrast agents such as iodine leads to new problems emerging, *e.g.* biological toxicity and dose local enhancement. The

purpose of this study was to find some effective setting strategies to mitigate the irradiation dose damage in an SRA experiment using a Monte Carlo simulation.

The depth dose curve and the dose enhancement ratio were estimated by Monte Carlo code *EGSnrc/DOSXYZnrc* simulation based on a 1-D mouse head model and a segmented voxel mouse head phantom to investigate the dose enhancement effect of the iodine contrast agent irradiated by a monochromatic synchrotron radiation source. The influences of iodine concentration, vessel width and depth, protection with and without a skull layer, and various incident X-ray energies were simulated. The dose enhancement effect and the absolute dose based on the monochromatic photon flux density at SSRF and the segmented voxel mouse phantom were evaluated.

The dose enhancement is mainly determined by the iodine concentration (IC) [see equation (1)]. For the relatively high velocity of blood flow with iodine solution, the microangiography usually has to start immediately after the contrast agent has been injected into the CCA. Thus, the local IC may be very high and so too the local dose. For example, at the

SSRF without shutter control, for 33.2 keV photons at  $6 \times 10^9$  photons  $\text{s}^{-1} \text{mm}^{-2}$  flux, even an IC of  $10 \text{ mg ml}^{-1} \text{s}^{-1}$  can lead to 2.71 Gy for the maximal and 1.92 Gy for the average VI doses, and its tolerance radiation times are 5.54/7.81 s for TD5/5 and 9.23/13.02 s for TD50/5, based on the human brain irradiated by a single dose (Emami *et al.*, 1991) (Table 1). The thin and younger mouse brain should certainly be more fragile than the human brain. Thus, an effective method to decrease the dose is to use the high- $Z$  contrast agent as little as possible and avoid irradiating the injected position site immediately after the contrast agent injection. Reducing the injection velocity of the contrast agent may also be a good route.

Schwenke *et al.* (2007) studied the imaging of the pulmonary circulation in a closed-chest rat using synchrotron radiation microangiography. They suggested using a dose of radiation of 1.4 mGy per frame at an exposure time of 2 ms with a maximum rate of 30 frames  $\text{s}^{-1}$  for up to 30 s, resulting in a total dose of 140 mGy in one scan of 100 consecutive frames with  $\sim 1 \times 10^{10}$  photons  $\text{s}^{-1} \text{mm}^{-2}$  flux at an energy of 33.2 keV. The shutter open time used in the study by Schwenke *et al.* (2007) was 2.6–3.0 ms per frame (here the higher value of 3.0 ms frame $^{-1}$  is assumed for caution), which means that the actual irradiation time and dose endured by the rat was 90 ms  $\text{s}^{-1}$  and 63.0 mGy  $\text{s}^{-1}$ , respectively. According to our calculation, however, even for an IC of  $10 \text{ mg ml}^{-1}$  at the SSRF, the VI dose can be up to 379.4 mGy  $\text{s}^{-1}$  for the maximum and 268.8 mGy  $\text{s}^{-1}$  for the mean. These doses are 6.02 and 4.27 times those reported by Schwenke *et al.* (2007). These differences could be in part because the total accumulative irradiation time per second with a shutter in dynamic imaging at the SSRF is 1.56 times that used by Schwenke *et al.* (2007). Another reason could be due to the fact that the work by Schwenke *et al.* only used the X-ray attenuation coefficient in water or tissue with the exponential attenuation formula to estimate the deposited energy and dose in the closed-chest rat, which is an analytical dose estimation method. This kind of analytical dose estimation method cannot account for the interaction of the secondary particles (*e.g.* electrons, photons) with the medium atoms, as well as the interaction of the X-rays with the iodine atoms in the mixture. However, it is an advantage of using the stochastic Monte Carlo method which can simulate the direct and indirect interaction of the X-ray photons with different atoms in the mixture. Fig. 2(c) also shows that the dose enhancement ratio of  $10 \text{ mgI ml}^{-1}$  is about 3.15, which is coincident with that reported by Schwenke *et al.* (2007).

Vascular resistance refers to resistance against blood flow for regulating blood flow and arterial pressure, which is determined primarily by changes in blood vessel diameters in small arteries and arterioles. Blood vessel wall motion regulates the changes in diameters. Thus, one of the more important things is to evaluate the effects of radiation on the blood vessel walls for these varied blood vessels. This work studied the dose enhancement effect of the iodine contrast agent with the variation of vessel width and depth based on a 1-D mouse head model. The study shows that the IC dose enhancement of a wall varies sharply [Figs. 2(a) and 2(b)], and is lower than

that in the blood vascular system for the dose buildup effect around the interface of different materials. In addition, compared with the flat vascular model in the 1-D mouse head model, the fluid pressure to the cylindrical blood vessel wall will also decrease slightly. However, this buildup effect is only evident at the scale of 20  $\mu\text{m}$ , and thus the inner wall of the blood vascular system still suffers from the damage of the IC dose enhancement.

Although the dose enhancement ratio depends little on the irradiation depth, the depth dose of low-energy X-ray photons itself decreases sharply with increasing depth. Thus, the fragile vessel incorporating iodine should avoid being closely irradiated.

The protection of the skull layer also cannot be ignored in SRA as even a 700  $\mu\text{m}$ -thick skull can decrease the dose by 10%. Thus, irradiating through a thin (or no) skull region should be avoided in SRA. Appending a thin equivalent material on the outside is also an alternative approach to decrease the dose in the brain vessel containing iodine.

The incident X-ray energy significantly affects the dose in the brain blood vessel containing iodine. To produce the higher-contrast effect using contrast agents, a lower or higher  $K$ -edge energy (*e.g.* 33.2 keV for iodine) is usually used. The medium attenuation decreases the incident X-ray energy; thus, an energy lower than the iodine  $K$ -edge is usually used to produce a good microangiography effect if the X-ray energy is 33.2 keV. However, using a slightly lower energy may be better in view of the dose protection. Even an energy of  $\pm 0.5$  keV could significantly enlarge the dose difference, especially for high iodine concentration. Thus, one of the effective methods of decreasing the dose is to use an incident X-ray energy that is as low as possible.

Xu (2013) investigated the effect of different synchrotron radiation X-ray energies (26, 28, 30, 32, 33, 33.7 and 34 keV) on image quality based on a simple three-tube model (PE8, Natsume Manufactory) with external and internal diameters of 0.5 mm and 0.2 mm to model the mouse coronary. The image quality was evaluated by the contrast ratio of the mean grey level of the whole image to that of the angiography region. Xu found that the image quality is very good for synchrotron radiation X-rays of 33–34 keV; however, the contrast ratio of the grey level sharply deteriorates from 33 to 32 keV. Xu verified this result based on an *in vivo* mouse experiment and concluded that 33 keV synchrotron radiation X-rays with 26  $\mu\text{m}$  spatial resolution and 50 ms time resolution could yield good image quality. Considering tissue attenuation of X-ray energy, some work regarded 33.7 keV as the  $K$ -edge energy of iodine (Xu, 2013). Thus, in fact, 33 keV is fairly lower than the iodine  $K$ -edge energy at a deeper depth. However, it has still displayed good image quality, especially after processing by some specific image enhancement technique. So, slightly decreasing the incident synchrotron radiation X-ray energy (*e.g.* 33 keV) will be a feasible method in irradiation protection.

The high X-ray flux density of a synchrotron radiation source is a double-edged sword. On one side it provides ample photons to improve the imaging resolution for micro-

angiography, even clearly displaying the micrometre order of vessel structures such as cerebral vasculature *in vivo* (Yuan *et al.*, 2011; Lu *et al.*, 2012; Kidoguchi *et al.*, 2006), whereas on the other side the  $6 \times 10^9$  photons  $\text{s}^{-1} \text{mm}^{-2}$  flux is a real challenge to the bearing capacity of living organisms. The entering dose rate can be up to  $31.87 \text{ Gy s}^{-1}$  for the first  $1 \mu\text{m}$  depth. Reducing the irradiation time or weakening the synchrotron radiation flux may be a necessary alternative.

Good synergetic and synchronous shuttering techniques are very important for irradiation protection in SRA. The synchrotron radiation source being shut off immediately between the imaging exposure interval of frames could effectively shorten the accumulative irradiation time. Generally, the image storage time is about tenfold that of the image exposure time, thus the actual tolerance irradiation time could be increased on a tenfold scale with a good synergetic shuttering technique. The shutter sometimes is not used for operation inconvenience in the rotation linkage between samples, detector and shutter *etc.* however which is very harmful for *in vivo* animal irradiation experiments.

Rotary irradiation such as multi-detector-row computed tomography is also a good way to decrease the local dose, as long as the SRA image registration is not an obstacle.

Fractional irradiation such as in cancer radiotherapy can effectively enhance the TD5/5 and the TD50/5 [e.g. 60 Gy for TD5/5 and 70 Gy for TD50/5 (Emami *et al.*, 1991)], which is also a practical solution.

The results of these studies were based only on a 1-D model and a segmented 28 g voxel mouse head phantom. Variations also have to be expected when using other sizes of phantoms. However, the DER was derived from the ratio of doses with and without iodine based on the same phantom. Thus, these results could be expected to be somewhat general. With respect to the limited penetration ability of low-energy photons emitted from a synchrotron radiation source, the current SRA has only been applicable to small-animal experiments such as those using mice, rats or rabbits; thus, this work has only simulated the small size of a 1-D head model and a voxel mouse head phantom.

## Acknowledgements

This work was supported by the Strategic Priority Research Program of the Chinese Academy of Sciences (XDA03040000) and Fundamental Research Funds for the Central Universities (2013HGXJ0193, J2014HGXJ0093, JZ2015HGXJ0184). Dr Xie Hong-Lan in Shanghai Synchrotron Radiation facility is highly appreciated for enlightening discussions.

## References

- Ayata, C., Shin, H. K., Dileköz, E., Atochin, D. N., Kashiwagi, S., Eikermann-Haerter, K. & Huang, P. L. (2013). *J. Cereb. Blood Flow Metab.* **33**, 954–962.
- Castelli, E. *et al.* (2011). *Radiology*, **259**, 684–694.
- Chien, C. C., Wang, C. H., Wang, C. L., Li, E. R., Lee, K. H., Hwu, Y., Lin, C. Y., Chang, S. J., Yang, C. S., Petibois, C. & Margaritondo, G. (2010). *Anal. Bioanal. Chem.* **397**, 2109–2116.
- Deak, P. D., Smal, Y. & Kalender, W. A. (2010). *Radiology*, **257**, 158–166.
- Dogdas, B., Stout, D., Chatziioannou, A. & Leahy, R. M. (2007). *Phys. Med. Biol.* **52**, 577–587.
- Emami, B., Lyman, J., Brown, A., Cola, L., Goitein, M., Munzenrider, J. E., Shank, B., Solin, L. J. & Wesson, M. (1991). *Int. J. Radiat. Oncol. Biol. Phys.* **21**, 109–122.
- Kawrakow, I., Mainegra-Hing, E., Rogers, D. W. O., Tessier, F. & Walters, B. R. B. (2010). NRCC Report PIRS-701. Ottawa: NRCC.
- Keyriläinen, J., Fernández, M., Karjalainen-Lindsberg, M.-L., Virkkunen, P., Leidenius, M., von Smitten, K., Sipilä, P., Fiedler, S., Suhonen, S., Suortti, P. & Bravin, A. (2008). *Radiology*, **249**, 321–327.
- Kidoguchi, K., Tamaki, M., Mizobe, T., Koyama, J., Kondoh, T., Kohmura, E., Sakurai, T., Yokono, K. & Umetani, K. (2006). *Stroke*, **37**, 1856–1861.
- Lin, H., Cai, J., Dai, Y., Jing, J., Pei, X., Cao, R. & Chen, C. (2013). *Med. Phys.* **40**, 207.
- Lin, H., Jing, J., Cai, J. F. & Xu, L. F. (2012). *Cancer Biother. Radiopharm.* **27**, 344–352.
- Lin, X., Miao, P., Wang, J., Yuan, F., Guan, Y., Tang, Y., He, X., Wang, Y. & Yang, G. (2013). *PLoS One*, **8**, e75561.
- Longo, M., Blandino, A., Ascenti, G., Ricciardi, G. K., Granata, F. & Vinci, S. (2002). *Neuroradiology*, **44**, 689–694.
- Lu, H., Wang, Y., He, X., Yuan, F., Lin, X., Xie, B., Tang, G., Huang, J., Tang, Y., Jin, K., Chen, S. & Yang, G. Y. (2012). *Stroke*, **43**, 838–843.
- Miao, P., Lin, X., Feng, S., Xie, B., Zhang, Q., Liu, C. & Yang, G. (2014). *Laser Phys.* **24**, 085603.
- Ota, R., Kurihara, C., Tsou, T. L., Young, W. L., Yeghiazarians, Y., Chang, M., Mobashery, S., Sakamoto, A. & Hashimoto, T. (2009). *J. Cereb. Blood Flow Metab.* **29**, 1547–1558.
- Piepgras, A., Thomé, C. & Schmiedek, P. (1995). *Stroke*, **26**, 2347–2352.
- Saltybaeva, N., Jafari, M. E., Hupfer, M. & Kalender, W. A. (2014). *Radiology*, **273**, 153–159.
- Schwenke, D. O., Pearson, J. T., Kangawa, K., Umetani, K. & Shirai, M. (2008). *J. Appl. Physiol.* **104**, 88–96.
- Schwenke, D. O., Pearson, J. T., Umetani, K., Kangawa, K. & Shirai, M. (2007). *J. Appl. Physiol.* **102**, 787–793.
- Stout, D., Chow, P., Silverman, R., Leahy, R. M., Lewis, X., Gambhir, S. & Chatziioannou, A. (2002). *Mol. Imaging Biol.* **4**, S27.
- Walters, B., Kawrakow, I. & Rogers, D. W. O. (2011). NRCC Report PIRS-794revB. Ottawa: NRCC.
- Wang, Z., Luo, W., Zhou, F., Li, P. & Luo, Q. (2012). *J. Biomed. Opt.* **17**, 125001.
- Xu, L. J. (2013). Doctoral dissertation, Shanghai Jiao Tong University, People's Republic of China.
- Yuan, F., Tang, Y., Lin, X., Xi, Y., Guan, Y., Xiao, T., Chen, J., Zhang, Z., Yang, G. Y. & Wang, Y. (2011). *J. Neurotrauma*, **29**, 1499–1505.